A black hole detected in the young massive LMC cluster NGC 1850

S. Saracino [©],[1]★ S. Kamann [©],[1] M. G. Guarcello,[2] C. Usher [©],[3] N. Bastian,[1,4,5] I. Cabrera-Ziri,[6]
M. Gieles [©],[7,8] S. Dreizler,[9] G. S. Da Costa [©],[10] T.-O. Husser[9] and V. Hénault-Brunet [©][11]

[1]*Astrophysics Research Institute, Liverpool John Moores University, 146 Brownlow Hill, Liverpool L3 5RF, UK*
[2]*Osservatorio Astronomico di Palermo, Piazza del Parlamento 1, I-90134, Palermo, Italy*
[3]*Department of Astronomy, Oskar Klein Centre, Stockholm University, AlbaNova University Center, SE-106 91 Stockholm, Sweden*
[4]*Donostia International Physics Center (DIPC), Paseo Manuel de Lardizabal, 4, 20018, Donostia-San Sebastián, Guipuzkoa, Spain*
[5]*IKERBASQUE, Basque Foundation for Science, E-48013 Bilbao, Spain*
[6]*Astronomisches Rechen-Institut, Zentrum für Astronomie der Universität Heidelberg, Mönchhofstraße 12-14, D-69120 Heidelberg, Germany*
[7]*ICREA, Pg. Lluís Companys 23, E-08010 Barcelona, Spain*
[8]*Institut de Ciències del Cosmos (ICCUB), Universitat de Barcelona (IEEC-UB), Martí i Franquès 1, E-08028 Barcelona, Spain*
[9]*Institute for Astrophysics, Georg-August-University Göttingen, Friedrich-Hund-Platz 1, D-37077 Göttingen, Germany*
[10]*Research School of Astronomy and Astrophysics, Australian National University, Canberra, ACT 0200, Australia*
[11]*Department of Astronomy and Physics, Saint Mary's University, 923 Robie Street, Halifax, NS B3H 3C 3, Canada*

ABSTRACT
We report on the detection of a black hole (NGC 1850 BH1) in the $\sim$100-Myr-old massive cluster NGC 1850 in the Large Magellanic Cloud. It is in a binary system with a main-sequence turn-off star ($4.9 \pm 0.4\,M_\odot$), which is starting to fill its Roche lobe and is becoming distorted. Using 17 epochs of Very Large Telescope/Multi-Unit Spectroscopic Explorer observations, we detected radial velocity variations exceeding $300\,km\,s^{-1}$ associated with the target star, linked to the ellipsoidal variations measured by the fourth phase of the Optical Gravitational Lensing Experiment in the optical bands. Under the assumption of a semidetached system, the simultaneous modelling of radial velocity and light curves constrains the orbital inclination of the binary to $38° \pm 2°$, resulting in a true mass of the unseen companion of $11.1^{+2.1}_{-2.4}\,M_\odot$. This represents the first direct dynamical detection of a black hole in a young massive cluster, opening up the possibility of studying the initial mass function and the early dynamical evolution of such compact objects in high-density environments.

Key words: techniques: imaging spectroscopy – techniques: radial velocities – binaries: spectroscopic – globular clusters: individual: NGC 1850 – galaxies: photometry.

1 INTRODUCTION

The tremendous number (50 in GWTC-2) of gravitational waves (GWs) detected by the Laser Interferometer Gravitational-Wave Observatory (LIGO) since 2015 (Abbott et al. 2016a, b) gives a sense of how urgent and important it is to characterize the properties of their progenitors – that is, dense compact objects such as neutron stars (NSs) and black holes (BHs) – and to study both their formation and evolutionary channels. Moreover, the recent discovery of a BH with a mass of $\sim 150\,M_\odot$ (the first secure detection of an intermediate-mass BH; Abbott 2020a, b) as the coalescence product of two very massive BHs ($60\,M_\odot$ and $85\,M_\odot$, respectively) has challenged our understanding of stellar evolution in massive stars (Vink et al. 2021). This has moved the focus to high-density environments such as massive stellar clusters, where merger cascades are most likely to occur (see the recent review by Gerosa & Fishbach 2021). However, BHs are elusive objects, and apart from GW emission of coalescing binary BHs, we have only two ways to detect them: indirectly, via the radio, X-ray or gamma-ray emissions of matter accreting on

to them, or directly, by studying the orbital motion of a visible companion orbiting around it in a binary system. Over the past decades, there have been numerous indirect detections of BHs as members of binaries with luminous companions, and many of these binary candidates have been identified through X-ray and radio observations of accreting systems (see Cowley 1992 as an example). The first BHs in old globular clusters (GCs) were also detected in this way (e.g. Maccarone et al. 2007; Strader et al. 2012; Chomiuk et al. 2013; Miller-Jones et al. 2015), challenging the classical idea that most BHs are expected to be ejected from the cluster on relatively short time-scales ($<10^9$ yr; Kulkarni, Hut & McMillan 1993). Only a few direct dynamical detections of non-interacting BHs have been made so far in star clusters (in the $\sim$12-Gyr-old NGC 3201; Giesers et al. 2018, 2019) because of observational limitations (i.e. the need for high spatial and spectral resolution in crowded fields and multiple epochs), so we know very little about the initial mass distribution of BHs and their early dynamical evolution. In addition to these signals of individual BHs, other observables may point at populations of stellar BHs in star clusters, such as the evolution of core radius with age (Mackey et al. 2007, 2008), the absence of mass segregation of stars (Peuten et al. 2016; Alessandrini et al. 2016; Weatherford et al. 2020), the central mass-to-light ratio of Omega Cen (Baumgardt

★ E-mail: s.saracino@ljmu.ac.uk

et al. 2019; Zocchi, Gieles & Hénault-Brunet 2019), the core over half-light radius (Askar, Arca Sedda & Giersz 2018; Kremer et al. 2020) and the presence of tidal tails (Gieles et al. 2021). Young massive clusters (< a few Gyr) are the best places to look in order to shed new light on the field. Indeed, the detection of BHs can provide crucial constraints on their retention fraction after supernova natal kicks (before significant dynamical evolution and dynamical ejections have taken place); this is a major uncertainty in GC models. However, to the best of our knowledge, no claims have been made so far about a direct dynamical detection of a BH in these objects.

We are currently conducting a systematic search for stellar-mass BHs in two young massive stellar clusters in the Large Magellanic Cloud (LMC) by exploiting multi-epoch Multi-Unit Spectroscopic Explorer (MUSE; Bacon et al. 2010) observations taken at the ESO Very Large Telescope (VLT), through the monitoring of radial velocity variations. This approach is highly sensitive to the detection of stellar companions of massive objects. Here we present the first outcome of the survey: the discovery of the first BH in NGC 1850, a massive ($M \sim 10^5\,M_\odot$; McLaughlin & van der Marel 2005) $\sim$100-Myr-old cluster. This is also one of the rare cases where the true BH mass can be estimated, as the inclination of the binary is well constrained from photometric light curves provided by the Optical Gravitational Lensing Experiment (OGLE; Udalski et al. 1992), given an assumed configuration for the system.

2 OBSERVATIONS AND DATA REDUCTION

We observed NGC 1850 with MUSE in wide-field mode (WFM; programmes 0102.D-0268 and 106.216T.001; PI: Bastian), taking advantage of the adaptive optics (AO) module, which provides a substantial improvement in terms of the spatial resolution of the images. In WFM, MUSE covers a field of view (FOV) of 1×1 arcmin^2 at a spatial sampling of 0.2 arcsec. Each spaxel records a spectrum from 470 to 930 nm at a (nearly) constant FWHM of 0.25 nm, corresponding to a spectral resolution between 1700 at the blue end and 3500 at the red end of the spectral range. As demonstrated by Kamann et al. (2016) using telluric absorption features, the wavelength calibration of MUSE is stable to 1 km s^{-1}, both across the FOV and in between observations.

The observations consist of two pointings, separated by about 50 arcsec. One is centred on the cluster core, and the other samples a slightly outer region (hereafter, we refer to these as centre and outer pointings). These data span a time baseline of almost 2 yr, with a time sampling between individual epochs ranging from 1 h to several months. This configuration ensures our sensitivity to binaries over a wide range of orbital periods within the cluster. Although a detailed description of the binary content of NGC 1850 will be presented in a forthcoming paper, we mention here that for every single bright source within either MUSE FOV we have a sample of 16 extracted spectra with a good signal-to-noise ratio (S/N), which goes up to 32 for stars in the overlapping region between centre and outer pointings.

We used the standard ESO MUSE pipeline to reduce the MUSE raw data (ESO Reflex; Weilbacher et al. 2020), while the extraction of individual stellar spectra was performed with the latest version of PAMPELMUSE (Kamann, Wisotzki & Roth 2013), based on a technique of fitting the point spread function (PSF) using the combined spatial and spectral information. For a proper extraction of the spectra, high spatial resolution photometry is needed as a reference. We took advantage of archival *Hubble Space Telescope* (*HST*) observations of NGC 1850, taken with the WFC3 camera during programmes 14069 (PI: Bastian) and 14174 (PI: Goudfrooij).

The data, which consist of images in ultraviolet to optical filters, were analysed using a standard PSF-fitting technique within the photometric software DOLPHOT (Dolphin 2016). The magnitudes of bright stars, saturated in almost all the long exposures, were recovered using the shortest exposure (7 s) in F814W. This catalogue was then used as a reference for the extraction process within PAMPELMUSE.

3 PHOTOMETRIC AND SPECTROSCOPIC ANALYSIS

Binary stars in GCs are expected to be in tight orbits in order to survive in such dense environments. This means that even in high spatial resolution images (e.g. *HST*), the two components should not be resolved. One possibility to detect these compact sources is via a systematic search for radial velocity variations, reflecting the precise orbital motion of one star around the other. Except for the case where both stars have similar brightness, the extracted spectrum will be always dominated by one of the stars. This approach is extremely powerful as it enables us to distinguish between luminous and dark companions. While a few interesting targets have been identified in this way in NGC 1850, here we devote our attention to a specific target star in the sample, showing radial velocity variations exceeding 300 km s^{-1}, a clear footprint of an underlying binary system and a massive (likely dark) companion.

The target star, which has RA = 77°1945 and Dec. = −68°7655 [05:08:46.7−68:45:55.6], is located at a distance of about 18.8 arcsec (4.47 pc) from the centre of NGC 1850 and within its effective radius $r_{eff} = 20.5 \pm 1.4$ arcsec (4.97 ± 0.35 pc; Correnti et al. 2017). The position in the MUSE FOV is shown in Fig. 1(a), while Fig. 1(b) shows a 16 x 16 arcsec^2 zoom of the region around the star from *HST* in the F814W band. The star is relatively bright, 16.7 mag in the F438W filter (16.6 mag in F814W), and located on the main-sequence turn-off (MSTO) of NGC 1850 in the *HST*/WFC3 colour–magnitude diagram (CMD; see Fig. 1, right-hand panel). We adopt a distance modulus of $(m - M)_0 = 18.45$ mag, an extinction E(B − V) = 0.1 and an age of the cluster of $\sim$100 Myr (Bastian et al. 2016). This allows us to determine the stellar mass of the visible star, as well as a first guess for the effective temperature T_{eff}, surface gravity log(g) and metallicity, from the comparison with up-to-date theoretical models.[1] Because stars in clusters of this age show significant rotation, we have used a set of rotating and non-rotating MESA Isochrones and Stellar Tracks (MIST) models (age = 100 Myr and Fe/H = −0.2; Choi et al. 2016; Gossage et al. 2019), deriving a mass for the visible component of $\sim 4.9\,M_\odot$. The right-hand panel of Fig. 1 shows isochrones with different rotation rates, and the difference in mass at the magnitude level of the target star does not exceed $\pm 0.25\,M_\odot$. To evaluate the effect introduced by errors on the adopted parameters, we simulated a synthetic population of 2×10^5 stars, assuming Gaussian distributions of 100 ± 20 Myr, 0.1 ± 0.03 mag, 18.45 ± 0.05 and -0.20 ± 0.25 for age, extinction, distance modulus and metallicity, respectively. The mass distribution for stars at the MSTO level, according to the MIST isochrones, peaks at 4.9 $M_\odot$, with $\sigma = 0.3\,M_\odot$. Once photometric errors and different rotation rates are also taken into account, the uncertainty on the target star mass is $\sim \pm 0.4\,M_\odot$.

---

[1]The models adopted are for the evolution of a single star, but it is likely that our target star had some form of interaction with its companion in the past. This may have an impact on the inferred mass, but we have not accounted for this effect, as binary evolution models are highly uncertain.
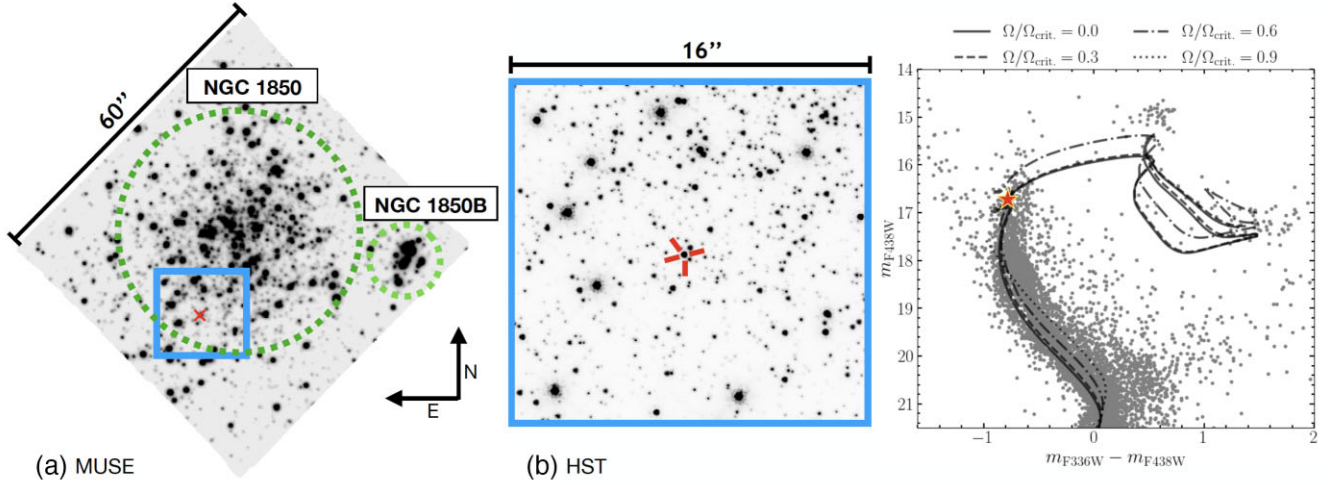
Figure 1. (a) The central pointing of NGC 1850, as seen by MUSE. Green circles identify the position of NGC 1850 as well as the younger cluster NGC 1850B. The red cross indicates the target star. An inset of the region in the blue square is displayed in panel (b). The image is taken from an archival *HST*/WFC3 image in the F814W band. The position of the target star is highlighted by red arrows. The right-hand panel shows an optical CMD of NGC 1850 from the archival *HST* data by Bastian et al. (2016). The target star position is shown as an orange star. Solid, dashed and dotted lines represent a set of rotating and non-rotating MIST models.

Table 1. MUSE radial velocity measurements for the target star and spectral S/N per pixel, averaged over the MUSE wavelength range. Radial velocities derived from spectra with S/N smaller than 10 are also included for completeness but they were excluded from the analysis to avoid introducing any spurious variability.

Time (MJD)	V_R (km s^{-1})	σV_R (km s^{-1})	S/N
58550.02867354	131.6	8.7	37.5
59201.25318966	151.9	8.9	36.1
59175.16932389	136.7	9.1	35.2
59203.14316930	401.1	9.0	34.4
58497.08534751	360.7	8.7	33.9
58556.01231551	135.0	10.4	33.8
59176.13916114	148.2	10.8	32.1
58498.15614836	364.4	10.7	31.6
59190.19805799	143.0	9.6	31.6
58553.01788807	399.5	9.8	28.7
59174.27808058	248.7	10.5	28.6
59251.14817479	139.6	11.8	27.5
59175.29610617	96.3	13.4	25.0
59176.30463698	178.9	12.6	24.7
59174.32203504	250.9	21.3	14.9
59177.30703879	340.7	21.9	13.8
58556.02541888	93.2	19.6	12.2
58550.04180262	147.7	20.2	9.1
58498.17027805	402.5	21.6	8.4
58553.03123202	435.9	37.3	4.8
59176.15348631	93.3	60.2	2.1
59175.17711612.	173.4	62.1	1.8

For the target star, we have a sample of 22 extracted spectra in total, with 17 having S/N greater than 10, while five show a lower S/N (see Table 1). The five spectra with low S/N come from the outer pointings, where this star is unfortunately located near one of the edges of the camera. In order to avoid introducing any spurious effects in the radial velocity data, we decided to discard these five spectra from the subsequent analysis.

To analyse the spectra, we made use of SPEXXY (Husser et al. 2016), software that determines radial velocities as well as stellar
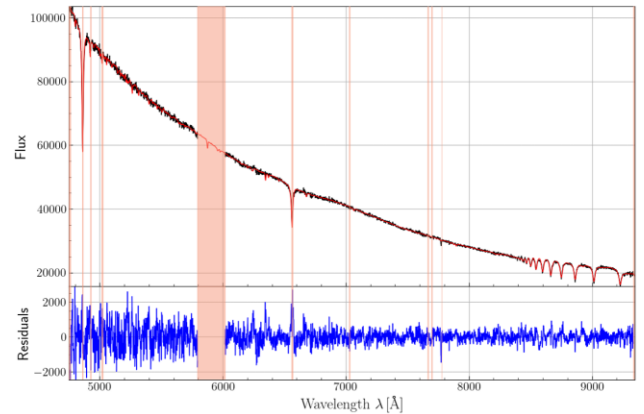
Figure 2. The combined, rest-framed, spectrum of our target star is shown in black. The best-fitting FERRE spectrum is overplotted in red. The bottom panel shows the residuals after subtracting the best-fitting model from the data. Pink-shaded regions are the spectral intervals masked out during the analysis, for example, because of the sodium emission of the laser in the AO mode and the diffuse nebulosity associated with NGC 1850B.

parameters (effective temperature, metallicity) using full-spectrum fitting against a set of templates. For the synthetic templates, we adopted the FERRE library (Allende Prieto et al. 2018). This library contains model stellar spectra for B-type stars, which are necessary when dealing with the young stars in NGC 1850. The FOV of NGC 1850 is contaminated by diffuse nebular emission, associated with the much younger (∼5 Myr) cluster NGC 1850B (shown as a small green circle in Fig. 1a), so all the spectral ranges that could potentially be contaminated by such an emission were masked out in our spectral analysis. The combined, rest-framed, spectrum of our target star is presented in black in Fig. 2, with the best-fitting model derived with SPEXXY overplotted in red. It looks like a standard B-type star spectrum but we find large changes in radial velocity of up to 307.9 km s^{-1} between epochs. The MUSE radial velocities and the corresponding S/N are listed in Table 1. We have also verified

that the variation we see in radial velocities comes effectively from the source, by analysing the only bright star (~0.5 mag fainter) in its proximity (RA = 77°.1943 and Dec. = −68°.7654, to the north-west with respect to the source in Fig. 1b) that could, in principle, contaminate its spectrum. This star, indeed, does not show any sign of variability,[2] therefore confirming that our target star is genuinely variable. By assuming a mean metallicity [Fe/H] = −0.20, consistent with previous estimates for the cluster iron content, and $\log(g) = 3.57$ as derived from the isochrones, we measured $T_{\rm eff} \sim 14\,500 \pm 500$ K, which is again expected for a B-type star.

4 RESULTS

4.1 Radial velocities

To constrain the orbital properties (the five standard Keplerian parameters plus the velocity semi-amplitude) of this binary system as well as to estimate the minimum mass of the unseen companion, we made use of THE JOKER (Price-Whelan et al. 2017, 2020). This software is a custom Monte Carlo sampler for sparse radial velocity measurements of two-body systems and can produce posterior samples for orbital parameters even when the likelihood function is poorly behaved. It is ideal in our case where only 17 radial velocity measurements, not equally sampled in time, are available. We generated 2^{29} prior samples[3] for the period range 0.3 d to 4096 d. We requested a maximum of 256 posterior samples, by assuming a Gaussian distribution for the cluster systemic velocity with 250 km s^{-1} and 5 km s^{-1} as mean and dispersion, respectively (Kamann et al. 2021). We found a unimodal solution with the binary system having a relatively short orbital period of $P = 5.0402$ d and moving almost on a circular orbit (very low eccentricity e). We ran THE JOKER again, this time limiting the possible solutions around the identified orbital period, specifically between 2 and 10 d, to increase the resolution of the grid. In addition, we also used the generalized Lomb–Scargle (GLS; Zechmeister & Kürster 2009) periodogram to analyse the radial velocity curve, and we found that aliasing is not a problem in this case, as a clear periodicity can be isolated robustly from the data. This is shown as a blue curve in Fig. 3, where a definite peak can be identified, with power close to 1. The overplotted orange curve instead shows the periodogram after the subtraction of the main peak.

To generate more posterior samples and to reliably estimate uncertainties on the orbital parameters, as well as a minimum mass for the unseen companion (by assuming an inclination of 90° for an orbit seen edge-on), we performed a Markov chain Monte Carlo (MCMC) analysis within THE JOKER. The (marginalized) posterior means and 1σ uncertainties are shown in Fig. 4 as corner plots, and are also listed in Table 2. As can be seen, the predicted minimum mass of the unseen source (i.e. fainter star) is $\sim 5.34\ \rm M_\odot$, already higher than the mass of the visible binary component (i.e. brighter star). The same lower limit on the mass of the unseen companion can be derived analytically from the observed velocity amplitude and period, by using the mass function in equations (1) and (2) of Ducati, Penteado & Turcati (2011), and assuming a mass for the observed binary component.

---

[2]It has a probability of 12 per cent of being variable, meaning that the radial velocity variations we observe for this star are not significant compared with the uncertainties of the individual RV measurements.

[3]We refer the reader to the documentation for JokerPrior.default for more details on the prior distributions.
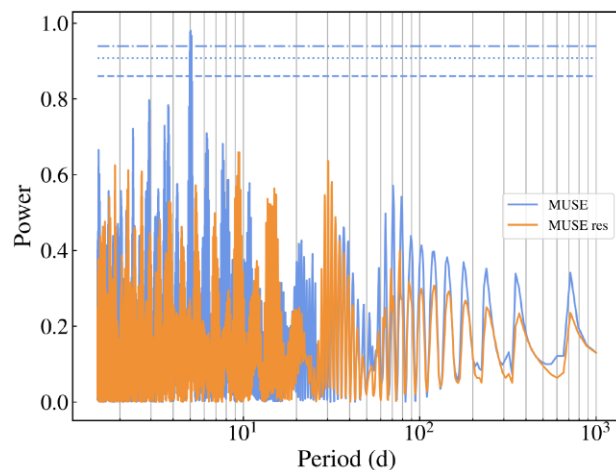
Figure 3. GLS periodogram of the MUSE radial velocities of the target star, before (blue curve) and after (orange curve) the subtraction of the main peak at ~5.04 d. Horizontal lines (from bottom to top) indicate the power corresponding to a 1 per cent, 0.1 per cent and 0.01 per cent false alarm probability. All peaks under these curves have a high probability of being unreal.
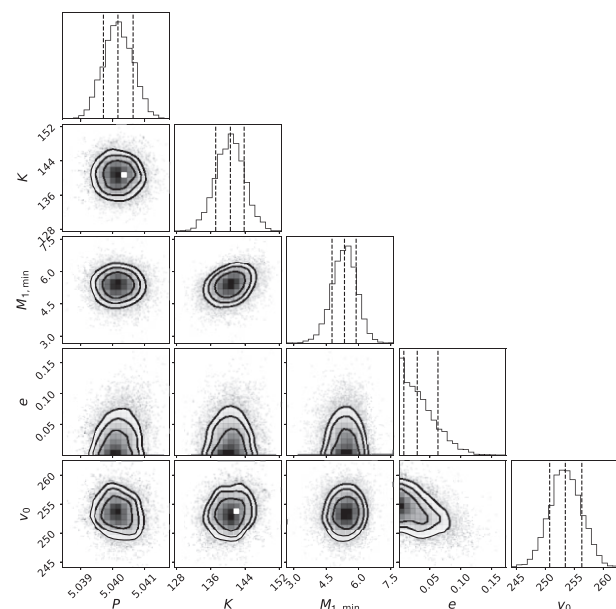
Figure 4. Corner plots showing the one- and two-dimensional projections of the posterior probability distributions for all the parameters of the binary system derived from THE JOKER + MCMC: Period P (d), velocity semi-amplitude K (km s^{-1}), minimum unseen companion mass $M_{\rm 1,\,min}$ (M$_\odot$), eccentricity e and barycentre velocity v_0 (km s^{-1}). The contours show the 1σ, 2σ and 3σ levels.

This result, corroborated by visual inspection of both the CMD and the MUSE spectra, represents the first clear indication that this object is compact and dark rather than luminous, and in particular a stellar-mass BH, because its estimated minimum mass is higher than any possible NS ($M \sim 3$M$_\odot$; Lattimer & Prakash 2001). Furthermore, the fitted radial velocity of the binary barycentre ($v_0 \sim 253$ km s^{-1}) is in good agreement with the systemic velocity of the cluster, meaning

Table 2. Binary system properties, from THE JOKER and PHOEBE.

THE JOKER + MCMC	
Period P	5.0402 ± 0.0004 d
Velocity semi-amplitude K	$140.40^{+3.31}_{-3.42}$ km s^{-1}
Barycentric radial velocity v_0	$253.30^{+2.59}_{-2.44}$ km s^{-1}
Minimum companion mass $M_1 \sin(i)$	$5.34^{+0.55}_{-0.59}$ M$_\odot$
PHOEBE + MCMC	
Inclination i	$37.9^{+2.2}_{-1.9}$ deg
Mass ratio q	$0.45^{+0.14}_{-0.07}$
Eccentricity e	$0.029^{+0.010}_{-0.014}$
Argument of periastron ω_0	222^{+27}_{-41} deg
Secondary mass M_2	$4.98^{+0.10}_{-0.10}$ M$_\odot$
Effective temperature $T_{\rm eff}$	14353^{+83}_{-119} K
Semimajor axis a	$31.2^{+1.3}_{-1.6}$ R$_\odot$
Companion mass M_1	$11.1^{+2.1}_{-2.4}$ M$_\odot$

that there is a high probability that the target star is a cluster member.[4] To verify that this is not a consequence of our prior (which assumed a Gaussian distribution of velocities around the cluster mean), we ran THE JOKER again by assuming a velocity distribution similar to that of the LMC field in the region, sensibly increasing the number of possible solutions for the binary. We found that, even in this case, the software converges to the same best-fitting solution for the radial velocity barycentre, confirming that this binary is most likely a cluster member.

4.2 Light curves

Radial velocity measurements alone cannot provide us with any constraints on the inclination of the orbit of the binary system, so only a minimum mass for the unseen companion can be estimated. Only in special configurations (i.e. eclipsing binaries), where photometric light curves are also available, can the inclination of the orbit be inferred in a reliable way.

Fortunately, this star is included in the catalogue of LMC variable stars compiled by OGLE (third release) as OGLE-LMC-DPV-039 and classified as double periodic variable (Poleski et al. 2010). It shows two periods, a shorter one at 5.040495 d and a ∼30 times longer one at ∼156 d. This class of objects is enigmatic; in fact, if the shortest period is associated with the orbital motion, the origin of the longer periodic variation is still unclear (Mennickent et al. 2003). The orbital period of our target star derived by THE JOKER ($5.0402^{+0.0004}_{-0.0004}$ d) using radial velocity variations perfectly matches the short period found photometrically by OGLE, confirming that we are indeed looking at the same star. This star is also in the OGLE fourth release as OGLE-LMC-ECL-29851 and Pawlak et al. (2016) additionally classified it as an eclipsing binary. By visually inspecting the light curves, we were unable to clearly see an eclipse in the data, and by applying the GLS periodogram to the light curves, we identified a significant peak at about 2.52 d, corresponding to $P_{\rm orb}/2$, with no peaks around the orbital period. This is an unambiguous property of an ellipsoidal variable, where the light curves show two maxima and minima per orbit – two cycles for every one cycle

of the velocity curve. This finding could then suggest that the star was misclassified as an eclipsing binary, rather than an ellipsoidal variable, in the OGLE-IV catalogue.

By using the latest version of PHOEBE (v2.3; Conroy et al. 2020), a software for modelling the light and radial velocity curves of binaries, we were able to put further constraints on the system and also to confirm previous findings.

(i) This system is, in fact, not an eclipsing binary as no eclipses are present in the light curves. Given how symmetrical the light curves are, if the system were an eclipsing binary, the two stars would have similar radii and luminosities. However, the star we see is clearly a single lined binary (SB1) so it must be significantly brighter than its unseen companion.

(ii) It is most likely in a semidetached binary system with the visible star filling its Roche lobe. In this configuration, the B-type star becomes distorted by the tidal influence of its orbiting companion and it takes on an elongated or ellipsoidal shape, becoming an ellipsoidal variable. The light variability we see in the OGLE light curves is caused mainly by the change in the apparent surface area as the star orbits around its companion. This peculiar feature has been extensively used in the literature, mainly for X-ray binaries and cataclysmic variables (CVs), as it allows us to constrain the inclination of the systems and the masses of the compact objects (for more details, see Avni & Bahcall 1975; Orosz 2003).

(iii) An orbital inclination larger than 50° can be excluded with a high confidence level, for either a luminous or a dark companion, because the amplitude of the optical variations and the different depth between primary and secondary minima would not match the observational data (unless properties inconsistent with its position in the CMD are assumed for the B-type star). More details can be found in Appendix A. Given the configuration of the system, hereafter, we refer to the massive (probably dark) object as the primary component of the binary, while the B-type star, which has started to fill its Roche lobe, is referred to as the secondary component.

An orbital inclination of $i = 50°$ would imply a true mass for the companion higher than the minimum mass of 5.34 M$_\odot$ estimated by THE JOKER. This can be easily derived using equations (1) and (2) in Ducati et al. (2011), and hence the mass ratio $q = M_2/M_1$ of the binary would be much smaller than 1. This finding unequivocally rules out the possibility that the primary star could be luminous. If it is the case, indeed, it would be significantly brighter that the secondary, thus making it visible in the *HST* photometry, as well as in the MUSE spectra. Hence, we can firmly state that the primary star is a dark compact object, specifically a BH, the first directly dynamically detected in a young massive cluster to date, and we call it NGC 1850 BH1.

In Table 2 we present the main properties of the binary system we derived from PHOEBE. For the modelling of the radial velocity and light curves, we assigned the secondary star of the system the properties inferred from our analysis of the MUSE spectra, that is, a MSTO star with $T_{\rm eff} = 14\,500$ K and mass of 4.9 M$_\odot$. We used the option 'distortion method = none', which only accounts for the gravitational influence of the compact source (the BH companion) and we assume it is otherwise completely dark and transparent.[5] In particular, we performed an MCMC run (nwalkers = 48, niters = 1000, burnin = 226) with EMCEE (Foreman-Mackey et al. 2019)

---

[4]Unfortunately, while our target star is included in *Gaia* EDR3 (Brown et al. 2021), its astrometric solution fails several of the quality criteria listed in Fabricius et al. (2021), preventing us from reaching any conclusion about membership to the cluster from its proper motion.

[5]To simulate the presence of a BH we alternatively set the lowest temperature allowed by the code ($T_{\rm eff} = 300$ K) and a radius $R = 3 \times 10^{-6}$ R$_\odot$, as done in Jayasinghe et al. (2021), finding consistent results.
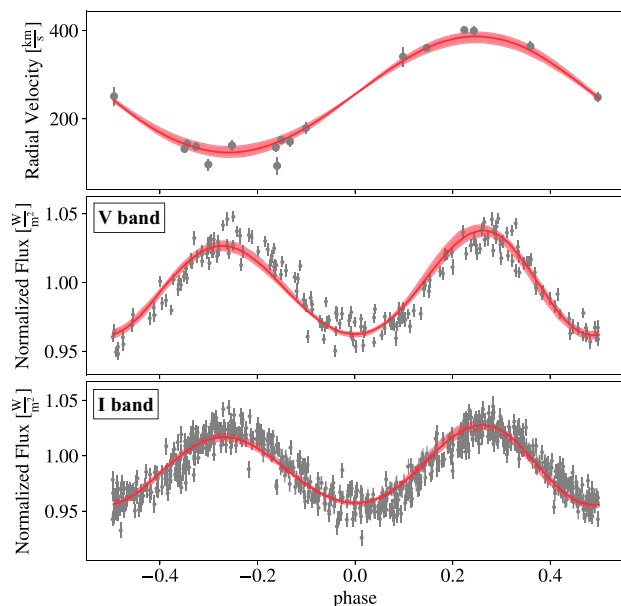
Figure 5. MUSE radial velocity curve (top) and OGLE light curves (centre panel, *V* band; bottom panel, *I* band) of the target star, phase-folded using a period of $P = 5.04$ d (see Table 2), are shown as grey dots. The red solid line represents the best-fitting model from PHOEBE. The red shaded areas indicate the 1σ uncertainties of the adopted parameters. The light curves show two maxima and minima per orbit – two cycles for every one cycle of the velocity curve − an unambiguous property of an ellipsoidal variable.

by fitting over the following parameters: inclination and period of the binary, mass ratio, eccentricity, argument of periastron and the mass and temperature of the B-type star. For those parameters that have been partially constrained by the previous analyses, we have imposed a Gaussian distribution around their values while for the others (i.e. orbital inclination and mass ratio) for which we do not have any constraints, we have assumed a uniform prior over the entire allowed range. The OGLE *V*- and *I*-band light curves, as well as the MUSE radial velocities, are presented as grey dots in Fig. 5, with the best-fitting model from PHOEBE overplotted as a solid red line. The red shaded areas represent the 1σ uncertainties from the MCMC run propagated toward the best-fitting model. The results ($i = 37.9^{+2.2\circ}_{-1.9}$ and $q = M_1/M_2 = 0.45^{+0.14}_{-0.07}$) are also shown as corner plots in Fig. 6, confirming the detection of a $11.1^{+2.1}_{-2.4}$ M$_\odot$ BH orbiting a MSTO star in NGC 1850. If the inclination of the system is indeed confirmed by further studies, this represents one of the few massive BHs detected so far and its relative mass uncertainty of 20 per cent (see Table 2) makes it one of the most accurate measurements available in the literature (Miller-Jones et al. 2021).

In Appendix B we test the hypothesis that the OGLE light curve of our target star might be contaminated by the flux of the bright source in its proximity (see Fig. 1b). We apply PHOEBE to the new light curves to understand how strongly this may affect the main physical properties of the binary system we have derived in this section. In summary, we obtain a slightly higher inclination and reduced mass of the BH of $9.2^{+1.6}_{-2.2}$ M$_\odot$, still within the uncertainties of the mass estimate given in Table 2.

5 SEARCHING FOR AN X-RAY COUNTERPART

Besides the strong evidence supporting the detection of a BH in NGC 1850 coming from the modelling of the radial velocity and

light curves, we have searched for independent probes to support our interpretation. When a BH is in a binary system, intense X-ray emission can arise from the accretion disc and the corona (e.g. Tanaka & Lewin 1995). The analysis of the X-ray emission from compact objects accreting material from their companions can thus shed important light on the accretion process, the outflow, and all the physical processes occurring in the system. In such a case, the emission can provide us with further evidence for the presence of a BH. Following the review by Remillard & McClintock (2006), the typically observed X-ray luminosity of BHs in binary systems in their quiescent state ranges from $10^{30.5}$ to $10^{33.5}$ erg s^{-1}, and their spectra are typically dominated by a power-law component with Γ between 1.5 and 2.1. Unfortunately, NGC 1850 is not the ideal target for X-ray studies as the cluster is compact and distant. Also, the region where the BH lies in the cluster is very close to the centre, where crowding represents a critical issue. Adopting a distance to NGC 1850 of 48 kpc, and using PIMMS v. 4.11,[6] the nominal ranges of X-ray luminosity and spectral index result in an expected count rate ranging from 6.2×10^{-7} to 5×10^{-4} counts s^{-1}. Except for the faintest limit, these count rates result in a detectable, even if faint, source in X-ray observations with an effective exposure of a few hundreds ks.

Among the available X-ray telescopes, only *Chandra*, with 13 ACIS-S observations within 10 arcmin from the location of the target star, for a total exposure time of 414 ks (P.I.: Williams and Portegies Zwart, the latter only for Obs. ID 3810; Williams et al. 2018), would be able to detect such a kind of emission. Table 3 shows the Obs.ID, the exposures and the aim points of the selected observations.

We first reprocessed the available primary data distribution files to produce new Level 2 event files using the CIAO script *chandra_repro* (Fruscione et al. 2006). We then followed the procedure described in the 'Correcting Absolute Astrometry' CIAO thread to correct the astrometry of each observation by aligning it on the deepest ACIS-S observation. The observations were thus merged using the *merge_obs* tool. Exposure maps in the broad (0.5–7.0 keV), soft (0.5–1.2 keV), medium (1.2–2.0 keV) and hard (2.0–7.0 keV) bands were calculated using the standard CIAO tools *asphist*, *mkinstmap* and *mkexpmap*. Fig. 7 shows an RGB image of the whole field and a zoom into the region where the target star, hence the candidate BH, and the supernova remnant (SNR) N103B are located.

A detailed detection and characterization of all the X-ray sources observed in the combined image is beyond the scope of this work. The strategy we adopted was, in fact, only aimed at investigating the presence (or absence) of a significant X-ray source at the position of the binary system and deriving its count rate. We first performed the source detection in the four bands using the CIAO tool *wavdetect*, with an adopted detection threshold of 10^{-4}. This choice resulted in 494 sources detected in the broad-band, 448 in the soft band, 467 in the medium band, and 339 in the hard band. After a visual inspection of the detections, a list of 1105 unique candidate sources was compiled. We then used the IDL software ACIS Extract (AE; Broos et al. 2010) with the aim of validating these sources. As no source has been found by *wavdetect* at the position of the BH, we inserted into the catalogue by hand a source at its position in order to let AE check the presence of any valid source at that position.

AE defines an individual photon extraction region for each source calculating the PSF at 1.5 keV, accounting for crowding by reducing the extraction region for crowded sources. The individual background is estimated by using an annular region centred on each source, with the inner radius equal to 1.1, 99 per cent of the PSF, and the outer

---

[6]https://cxc.harvard.edu/toolkit/pimms.jsp
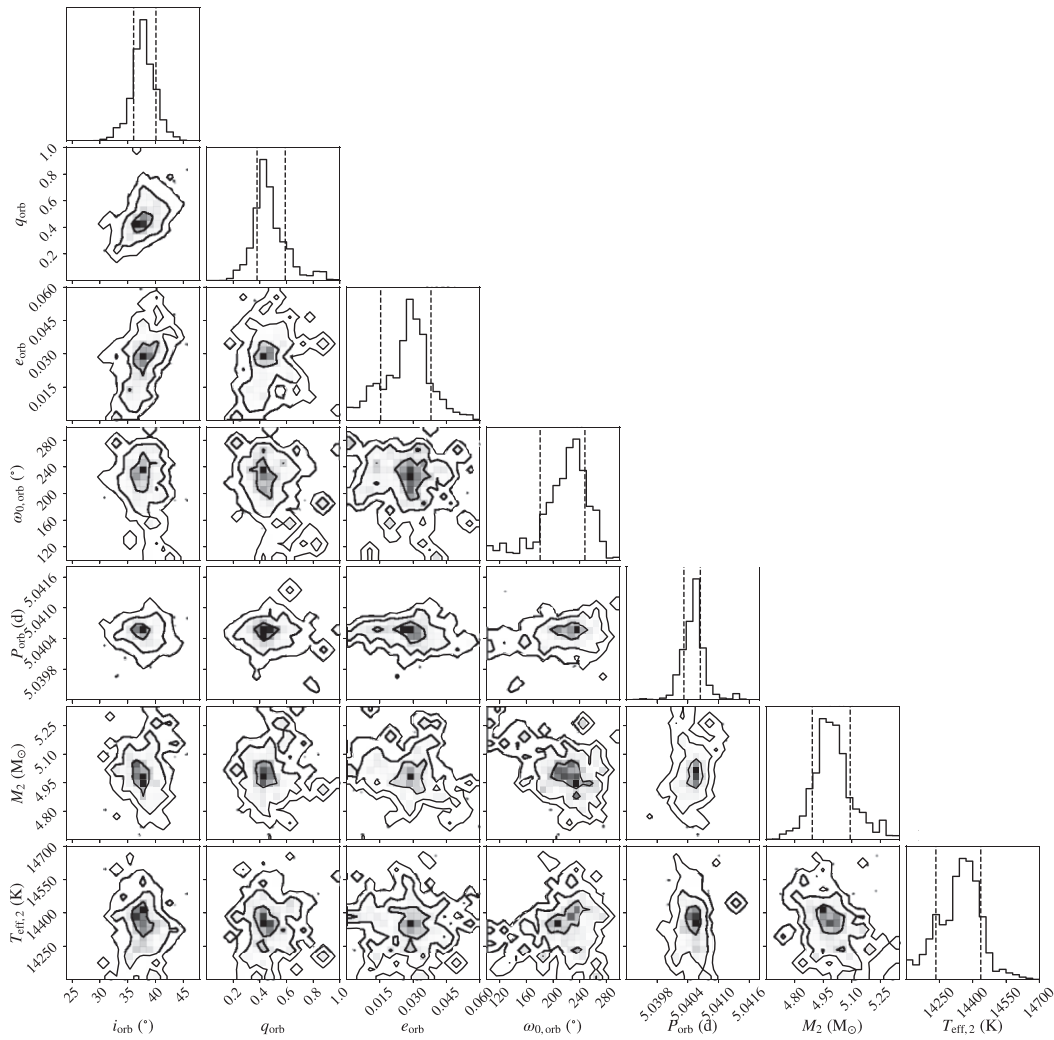
Figure 6. Corner plots showing the one- and two-dimensional projections of the posterior probability distributions for all the parameters of the binary system derived from PHOEBE + MCMC: inclination i ($°$), mass ratio q, eccentricity e, argument of periastron ω_0 ($°$), period P (d), mass (M$_\odot$) and T_{eff} (K) of the visible component. The contours correspond to the 1σ, 2σ and 3σ levels.

Table 3. *Chandra* observations of NGC 1850 analysed in this work.

Obs.ID	Exposure (ks)	RA (J2000)	Dec. (J2000)
3810	29.67	05:08:44	−68:45:36
18018	39.54	05:08:59	−68:43:34
18019	59.28	05:08:59	−68:43:34
18020	27.19	05:08:59	−68:43:34
19921	16.85	05:08:59	−68:43:34
19922	41.43	05:08:59	−68:43:34
19923	58.30	05:08:59	−68:43:34
20042	19.80	05:08:59	−68:43:34
20053	11.20	05:08:59	−68:43:34
20058	43.79	05:08:59	−68:43:34
20067	29.68	05:08:59	−68:43:34
20074	31.17	05:08:59	−68:43:34

radius large enough to encompass 100 background photons. For crowded regions, AE calculates the background from a model that accounts for the presence of nearby sources. In order to improve this model, the background must be estimated with several iterations.

We also used AE to correct source positions, adopting for on-axis sources ($\Theta \leq 5$ arcmin) the mean data position, which is obtained from the centroid of the extracted events, the correlation position for the off-axis sources, which is obtained by interpolating the PSF with the events distribution, and the maximum likelihood position for the crowded sources, which is calculated from the maximum likelihood image of source neighbourhood.

Once photon extraction and the estimate of the background was repeated after source relocation, we calculated the parameter *prob_no_source* (P_B), which provides the probability of the source being a background fluctuation and thus an estimate of its reliability (reliable sources typically have $P_B < 0.01$). At the position of the binary system, AE found a marginally reliable source in the soft band ($P_B = 0.003$[7]), which lies 0.45 arcsec to the east of the nominal position of the putative BH. By checking the *HST* image, no sources other than our binary system can be responsible for such an emission. Furthermore, the separation we observe between the optical and X-

[7]This roughly corresponds to the 35 per cent quantile of the P_B values in the soft band.
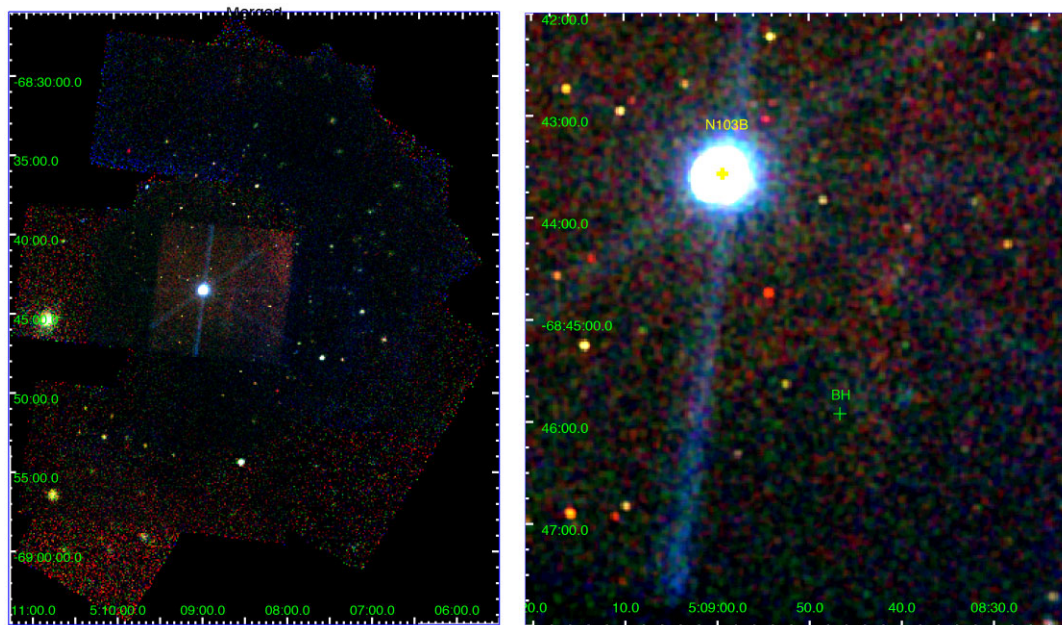
Figure 7. Merged RGB *Chandra*/ACIS-S images of NGC 1850 analysed in this work, with events in the hard band in red, medium band in green, and soft band in blue. The left panel shows the whole field, while the right panel is centred on the position of the candidate black hole and the bright SNR N103B.

ray counterpart is compatible with the astrometric offset between the two catalogues.[8] Despite its reliability, only 2.7 net counts are detected in the soft band (with a mean photon energy of 0.64 keV), which however corresponds to a count rate of 1.87×10^{-5} in the soft band, and thus, using PIMMS, to an X-ray luminosity of about 10^{33} erg s^{-1}. Thus, the result from the X-ray analysis would be consistent with a BH in a quiescent state. We emphasize, however, that a further characterization of the source is not possible, given its very few net counts.

6 DISCUSSION AND CONCLUSIONS

In this paper, we exploit MUSE radial velocities and OGLE-IV light curves to report the detection of a short period ($P = 5.04$ d) binary system in NGC 1850, made up of a ~ 4.9-M$_\odot$ MSTO star and a ~ 11-M$_\odot$ BH (NGC 1850 BH1), under the assumption of a semidetached configuration. The membership to NGC 1850 was established by analysing the barycentric radial velocity, the distance to the cluster centre, and the properties of the visible star (i.e. sharing the same turn-off mass and [Fe/H] as NGC 1850). The analysis of *Chandra* X-ray data revealed a faint but marginally reliable source at the location of the binary system, which would be consistent with the presence of a BH in a quiescent state.

Future studies of the cluster dynamics as well as the secondary stars' chemistry will help to shed light on the origin (primordial versus dynamically formed binary) of this intriguing system. The fate of the binary is, however, uncertain. Based on the evidence gathered so far, we speculate that the system will likely experience a Roche lobe overflow, as soon as the B-star evolves out of the main sequence. There will be a stable mass transfer and significant X-ray emission, generally leading to a widening of the binary. Mass transfer will likely end when most of the H envelope of the donor

star has either been transferred to the companion or been lost from the system, leaving an He star core (Soberman, Phinney & van den Heuvel 1997; Podsiadlowski 2008). If so, it will likely experience another phase of mass transfer (and X-ray emission) when the star burns He in shell, ending up as a BH + white dwarf system.

The detection of such a system has an important impact in different fields.

(i) *GC studies*. Finding a BH in a stellar cluster of just ~ 100 Myr represents the starting point in the construction of the BH initial mass function. Furthermore, it supports the search for the complete (dynamically detectable) population of BHs, allowing strict constraints to be placed on the BH retention fraction, a major uncertainty in GC models.

(ii) *The studies of binaries*. The physical properties of the visible star are very well constrained (e.g. mass, metallicity, age/evolutionary stage) by being a member of a massive cluster. This precision can help us to understand the physics responsible for the long-term periodic variations observed in the light curves of double periodic variables across the Milky Way and the Magellanic Clouds.

(iii) *The search for non-interacting (or weakly interacting) compact sources*. Our finding validates both the power and reliability of the radial velocity approach as an important tool for detecting these types of systems in different environments, especially in GCs. This result represents a proof of concept and will be extended to a diverse sample of GCs (at a variety of ages) in the future.

(iv) *BH mass measurement*. Very few mass measurements are available in the literature for NSs and BHs. They are mainly biased toward accreting binary systems selected via radio, X-ray and γ-ray data (see, e.g., Liu, van Paradijs & van den Heuvel 2006; Champion et al. 2008; Özel et al. 2010; Farr et al. 2011), and from the LIGO/Virgo detections of merging systems (see, e.g. Abbott et al. 2016b; Abbott 2017). Deriving the masses of non-interacting compact objects is a rare event – a few examples can be found in Thompson et al. (2019) and Jayasinghe et al. (2021) – but it really

---

[8]The mean astrometric offset between the two catalogues was measured using only the brightest sources. We identified 54 closest coincidences, adopting a tolerance radius of 10 arcsec.

becomes a novelty when they reside in GCs. This represents the very first step towards an unbiased characterization of the BH mass distribution in clusters.

Finally, although the radial velocity method presented here is not sensitive to binaries made up of two non-luminous components (such as BH–NS or BH–BH binaries), which are considered the main GWs emitters, similar studies are crucial both for understanding all the evolutionary phases in between a massive binary star and a binary BH, and for unveiling the population of BHs in massive clusters, as this is the most likely place in the Universe, due to the frequent dynamical encounters, where BH merger cascades could be possibly triggered

DATA AVAILABILITY

The MUSE data underlying the paper will be shared on reasonable request to the authors, while the *Chandra* data are available for download in the corresponding archive. The light curves are available on the OGLE website.

NOTE ADDED IN PROOF

The authors note that El-Badry & Burdge (2021) have offered an alternative explanation to the data presented in this paper.

REFERENCES

Abbott B. P. et al., 2016a, Phys. Rev. Lett., 116, 061102
Abbott B. P. et al., 2016b, ApJ, 818, L22
Abbott B. P. et al., 2017, Phys. Rev. Lett., 119, 161101
Abbott R. et al., 2020a, Phys. Rev. Lett., 125, 101102
Abbott R. et al., 2020b, ApJ, 900, L13
Alessandrini E., Lanzoni B., Ferraro F. R., Miocchi P., Vesperini E., 2016, ApJ, 833, 252
Allende Prieto C., Koesterke L., Hubeny I., Bautista M. A., Barklem P. S., Nahar S. N., 2018, A&A, 618, A25
Askar A., Arca Sedda M., Giersz M., 2018, MNRAS, 478, 1844
Avni Y., Bahcall J. N., 1975, ApJ, 197, 675
Bacon R. et al., 2010, Proc. SPIE, 7735, 773508
Bastian N. et al., 2016, MNRAS, 460, L20

Baumgardt H. et al., 2019, MNRAS, 488, 5340
Broos P. S., Townsley L. K., Feigelson E. D., Getman K. V., Bauer F. E., Garmire G. P., 2010, ApJ, 714, 1582
Brown A. G. A.Gaia Collaboration et al. (Gaia Collaboration) 2021, A&A, 649, A1
Champion D. J. et al., 2008, Science, 320, 1309
Choi J., Dotter A., Conroy C., Cantiello M., Paxton B., Johnson B. D., 2016, ApJ, 823, 102
Chomiuk L., Strader J., Maccarone T. J., Miller-Jones J. C. A., Heinke C., Noyola E., Seth A. C., Ransom S., 2013, ApJ, 777, 69
Conroy K. E. et al., 2020, ApJS, 250, 34
Correnti M., Goudfrooij P., Bellini A., Kalirai J. S., Puzia T. H., 2017, MNRAS, 467, 3628
Cowley A. P., 1992, ARA&A, 30, 287
Dolphin A., 2016, preprint (ascl:1608.013)
Ducati J. R., Penteado E. M., Turcati R., 2011, A&A, 525, A26
El-Badry K., Burdge K., 2021, preprint (arXiv:2111.07925)
Fabricius C. et al., 2021, A&A, 649, A5
Farr W. M., Sravan N., Cantrell A., Kreidberg L., Bailyn C. D., Mandel I., Kalogera V., 2011, ApJ, 741, 103
Foreman-Mackey D. et al., 2019, Journal of Open Source Software, 4, 1864
Fruscione A. et al., 2006, Proc. SPIE, 6270, 62701V
Gerosa D., Fishbach M., 2021, Nature Astronomy, 5, 749
Gieles M., Erkal D., Antonini F., Balbinot E., Peñarrubia J., 2021, Nature Astronomy, 5, 957
Giesers B. et al., 2018, MNRAS, 475, L15
Giesers B. et al., 2019, A&A, 632, A3
Gossage S. et al., 2019, ApJ, 887, 199
Husser T.-O. et al., 2016, A&A, 588, A148
Jayasinghe T. et al., 2021, MNRAS, 504, 2577
Kamann S. et al., 2016, A&A, 588, A149
Kamann S., Wisotzki L., Roth M. M., 2013, A&A, 549, A71
Kamann S., Bastian N., Usher C., Cabrera-Ziri I., Saracino S., 2021, MNRAS, 508, 2302
Kremer K. et al., 2020, ApJS, 247, 48
Kulkarni S. R., Hut P., McMillan S., 1993, Nature, 364, 421
Lattimer J. M., Prakash M., 2001, ApJ, 550, 426
Liu Q. Z., van Paradijs J., van den Heuvel E. P. J., 2006, A&A, 455, 1165
Maccarone T. J., Kundu A., Zepf S. E., Rhode K. L., 2007, Nature, 445, 183
Mackey A. D., Wilkinson M. I., Davies M. B., Gilmore G. F., 2007, MNRAS, 379, L40
Mackey A. D., Wilkinson M. I., Davies M. B., Gilmore G. F., 2008, MNRAS, 386, 65
McLaughlin D. E., van der Marel R. P., 2005, ApJS, 161, 304
Mennickent R., Pietrzyński G., Diaz M., Gieren W., 2003, A&A, 399, L47
Miller-Jones J. C. A. et al., 2015, MNRAS, 453, 3918
Miller-Jones J. C. A. et al., 2021, Science, 371, 1046
Orosz J. A., 2003, in van der Hucht K. A., Herrero A., Esteban C., eds, Proc. IAU Symp. No. 212, A Massive Star Odyssey: From Main Sequence to Supernova. Astron. Soc. Pac., San Francisco, p. 365
Özel F., Psaltis D., Narayan R., McClintock J. E., 2010, ApJ, 725, 1918
Pawlak M. et al., 2016, AcA, 66, 421
Peuten M., Zocchi A., Gieles M., Gualandris A., Hénault-Brunet V., 2016, MNRAS, 462, 2333
Podsiadlowski P., 2008, in Werner A., Rauch T., eds, ASP Conf. Ser. Vol. 391, Hydrogen-Deficient Stars. Astron. Soc. Pac., San Francisco, p. 323
Poleski R. et al., 2010, AcA, 60, 179
Price-Whelan A. M., Hogg D. W., Foreman-Mackey D., Rix H.-W., 2017, ApJ, 837, 20
Price-Whelan A. M. et al., 2020, ApJ, 895, 2
Remillard R. A., McClintock J. E., 2006, ARA&A, 44, 49
Sahu K., Deustua S., Sabbi E., 2014, WFC3/UVIS Photometric Transformations, Space Telescope WFC Instrument Science Report
Soberman G. E., Phinney E. S., van den Heuvel E. P. J., 1997, A&A, 327, 620
Strader J., Chomiuk L., Maccarone T. J., Miller-Jones J. C. A., Seth A. C., 2012, Nature, 490, 71

Tanaka Y., Lewin W. H. G., 1995, in Lewin W. H. G., Van Paradijs J., Van den Heuvel E. P. J., eds, X-ray Binaries. Cambridge Univ. Press, Cambridge, p. 126

Thompson T. A. et al., 2019, Science, 366, 637

Udalski A., Szymanski M., Kaluzny J., Kubiak M., Mateo M., 1992, AcA, 42, 253

Udalski A., Szymański M. K., Szymański G., 2015, AcA, 65, 1

Vink J. S., Higgins E. R., Sander A. A. C., Sabhahit G. N., 2021, MNRAS, 504, 146

Weatherford N. C., Chatterjee S., Kremer K., Rasio F. A., 2020, ApJ, 898, 162

Weilbacher P. M. et al., 2020, A&A, 641, A28

Williams B. J. et al., 2018, ApJ, 865, L13

Zechmeister M., Kürster M., 2009, A&A, 496, 577

Zocchi A., Gieles M., Hénault-Brunet V., 2019, MNRAS, 482, 4713

APPENDIX A: BINARY SYSTEM CONFIGURATION

The results reported in the main text for the inclination and the true mass of NGC 1850 BH1 are based on the assumption that the binary system is in a semidetached configuration. This assumption is strongly supported by the shape of the light curves themselves, as well as by the properties of the visible star derived from the comparison with up-to-date stellar evolutionary models. For completeness, however, we mention here that a best-fitting solution comparable (at least qualitatively) with the one presented in Fig. 6 can be obtained also under the assumption of a detached system, while assuming a lower value for $\log(g)$ (by $\sim$0.3 dex) compared to the one derived from our analysis. This value falls well outside the estimated uncertainties for the surface gravity of the star (if real, indeed, at fixed mass and T_{eff}, the star would appear much brighter than actually observed; see the right-hand panel of Fig. 1). For these reasons, we consider the detached configuration unlikely, so we adopted the semidetached configuration to model the light curves.

Nevertheless, this test has been extremely informative as it allowed us to obtain two important confirmations. (i) Even assuming a detached system, the inclination of the binary does not decrease by much ($\sim$10°–15°), so the companion still needs to be massive ($>8\,M_\odot$), and no other possibility other than a BH can be considered. (ii) An important source of uncertainty in modelling the light curves is the value adopted for $\log(g)$, which unfortunately we cannot measure directly from our MUSE spectra due to their low resolution. This modelling, indeed, would significantly benefit from this information coming from high-resolution data of the source, which are currently unavailable. These observations will help in discriminating between the two aforementioned configurations, and hence significantly reducing the uncertainties on both the inclination and the mass of the BH.

APPENDIX B: OGLE PHOTOMETRY AND ITS RESOLVING POWER

OGLE is one of the largest sky variability surveys but it has a lower spatial resolution compared with *HST*, so the photometric accuracy is limited in dense environments such as the innermost regions of star clusters. For this reason, there is a real probability that the OGLE photometry cannot resolve sources that are relatively close to each other ($\sim$0.5 arcsec) on the sky. This could be the case with our target star, which is located within the effective radius of NGC 1850 and has a relatively bright star in its proximity (see Fig. 1b). The offset of $\sim$0.4 mag measured in the *I* band between OGLE and *HST*, in fact, might be an indication of such a contamination. However, to definitively
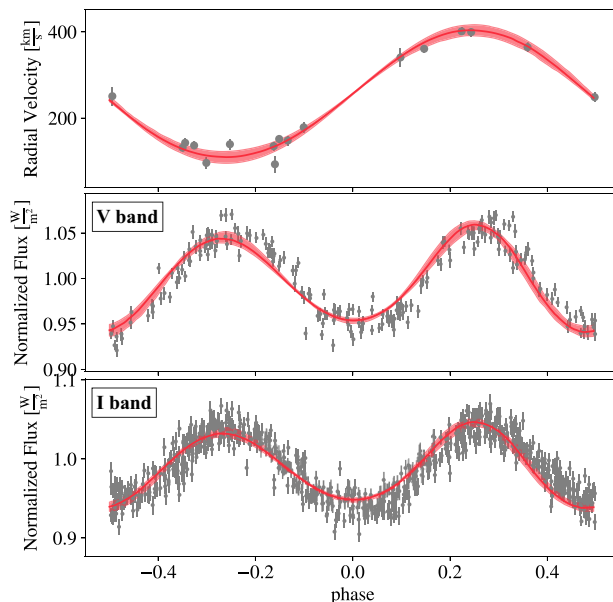
Figure B1. As in Fig. 5 but with the OGLE light curves decontaminated by the flux of the bright nearby star.

answer this question, we would need a light curve obtained from high spatial resolution photometry such as *HST*, which is currently unavailable.

To investigate the impact of a potential blend in the OGLE data on our results, we assumed the worst case, namely that OGLE was unable to resolve the two stars. We then subtracted the expected light contribution of the nearby star from every data point in the OGLE light curves. We used the *HST* zero points (Sahu, Deustua & Sabbi 2014) to convert the WFC3 F814W magnitude of the nearby star to the Johnson–Cousins *I* band.[9] The F555W band magnitude, which is not available in the *HST* catalogue, was instead deduced from the comparison with a MIST isochrone. After subtracting its flux from all measurements, we have derived new light curves, which show increased photometric modulation compared to the original ones (by $\sim$0.08–0.09 mag; see Fig. B1). Interestingly, after the subtraction, the aforementioned offset between OGLE and *HST* cancelled out almost perfectly.

As a further test, we recovered the *V*- and *I*-band magnitudes from all extracted spectra and created photometric light curves from the MUSE data, using one isolated nearby star from OGLE as calibrator. Again, the offset we observe relative to the magnitudes in the OGLE catalogue is consistent with what one would expect if the two stars are blended in the latter.

To derive the main physical properties of the binary and to see how they change when the original versus new light curves are adopted, we run PHOEBE again, as done in Section 4. The results are shown in Fig. B1 and Table B1 and can be directly compared with those in Fig. 5 and Table 2, respectively. As can be seen, assuming that the new light curves are the most reliable, then the inclination of the binary system would increase by $\sim$12° and the mass ratio q would be of 0.53, leading to a BH mass of $9.2^{+1.6}_{-2.2}\,M_\odot$, smaller than the previous estimate but still compatible within their uncertainties.

---

[9]The OGLE *I* and *V* bands are similar to the standard Johnson–Cousins *I* and *V* bands (Udalski, Szymański & Szymański 2015).

Table B1. Binary system properties from PHOEBE when decontaminated light curves are considered.

	PHOEBE + MCMC
Period P	5.0405 ± 0.0003 d
Inclination i	$49.6^{+4.5}_{-2.0}$ deg
Mass ratio q	$0.53^{+0.16}_{-0.07}$
Eccentricity e	$0.031^{+0.008}_{-0.007}$
Argument of periastron ω_0	209^{+35}_{-31} deg
Secondary mass M_2	$4.92^{+0.11}_{-0.15}$ M$_\odot$
Effective temperature $T_{\rm eff}$	14470^{+130}_{-120} K
Semimajor axis a	$29.8^{+1.2}_{-1.5}$ R$_\odot$
Companion mass M_1	$9.2^{+1.6}_{-2.2}$ M$_\odot$

This paper has been typeset from a TEX/LATEX file prepared by the author.